International Journal of Engineering & Technology, 7 (4.14) (2018) 555-559

International Journal of Engineering & Technology

Website: www.sciencepubco.com/index.php/IJET

Research paper

Electrical Properties of Li-based NASICON Structured Ceramic Electrolytes Substituted With Chromium

N. A. Mustaffa[1]*, N. S. Mohamed[2]

[1]Faculty of Applied Sciences, Universiti Teknologi MARA, 40450, Shah Alam, Selangor, Malaysia
[2] Centre for Foundation Studies in Science, University of Malaya, 50603 Kuala Lumpur
** Corresponding author E-mail: nuramalina@salam.uitm.edu.my*

Abstract

Electrical properties of Li - ion conducting $Li_{1+x}Cr_xSn_{2-x}(PO_4)_3$ ceramic electrolytes with $0 < x < 1$ were studied using electrical impedance spectroscopy in the frequency range of 1 Hz to 10 MHz at room temperature. Impedance analysis showed an increase in bulk and grain boundary conductivity with the increment of x up to $x = 0.7$. The highest bulk and grain boundary conductivity were 6.52×10^{-6} S cm^{-1} and 1.62×10^{-6} S cm^{-1} in the system of $Li_{1.7}Cr_{0.7}Sn_{1.3}(PO_4)_3$ at room temperature. The charge carrier concentration, mobile ion concentration, ionic hopping rate and ionic mobility were calculated by fitting the AC conductivity spectra. The ionic hopping rate and ionic mobility of the compound increased with the substitution of chromium due to the extra interstitial Li^+ ions in the system. Additionally, the highest conducting sample with $x = 0.7$ had a negligible electronic conductivity based on transference number measurements. These results imply that the $Li_{1+x}Cr_xSn_{2-x}(PO_4)_3$ electrolytes obtained in this work can be considered as future candidates for solid state electrolytes.

Keywords: *Lithium, NASICON, Electrolytes, Chromium, Conductivity*

1. Introduction

Rechargeable lithium ion batteries have dominated the consumer electronics market for decades due to their high specific energy, high efficiency and long life [1]. However, battery performance depends critically on the electrolytes used and the challenge now is the development of safer and more reliable solid electrolytes. Using stable inorganic solid state electrolyte to replace organic liquid electrolyte can significantly reduce safety risk of rechargeable batteries.

Solid state electrolytes such as Na-superionic conductor (NASICON)-structured is one of the most promising solid electrolytes and can be employed in solid-state batteries. Meanwhile, lithium analogous sodium superionic conductor (NASICON) structured also have received enormous attention after it was first discovered by Hong (1976) [2] and Goodenough et. al (1976) [3] in the system of $Na_{1+x}Zr_2Si_xP_{3-x}O_{12}$ [2]. Since then, various studies have focused on lithium analogous NASICON structured with the general formula $LiM_2P_3O_{12}$ with M = Ti [4, 5], Zr [6, 7],Sn [8-10] and etc. Lithium analogous NASICON structured electrolytes are made of a three−dimensional framework of TiO_6 octahedra and PO_4 tetrahedra with interstitial tunnels in which Li-ions can hop easily [11-13].

Lithium stannum phosphate, $LiSn_2P_3O_{12}$ is a Li^+ ion conductor that shows NASICON type structure and the least studied in the NASICON family [14-17]. The main challenge was to obtain high ionic conductivity for $LiSn_2P_3O_{12}$ compound as Martinez-Juarez and co-workers (1997) and Lazarraga and co-reserachers (2004) have reported that $LiSn_2P_3O_{12}$ having low ionic conductivity of ~ 10^{-10} S cm^{-1} [18]. So, in order to enhance the ionic conductivity of the NASICONs compound, partial substitution can be carried out by partially substituting Sn^{4+} ions with trivalent ions such as Al^{3+}, Cr^{3+} or Fe^{3+}. It was systematically shown for the first time by Aono et al. [19]. These authors reported that the increase of ionic conductivity observed in $Li_{1+x}M_{3+x}Ti_{2-x}(PO_4)_3$ compounds was due both to the increase of the lithium content and to a better connectivity of the grains caused by a density increase associated to segregated phases in grain boundaries acting as binders. This is probably the origin of the high ionic conductivity of almost 10^{-3} S cm^{-1} at room temperature found for $Li_{1.3}Al_{0.3}Ti_{1.7}(PO_4)_3$[20]. So our present study focused on enhancing the ionic conductivity of $LiSn_2P_3O_{12}$ parent compound by partially substituting Sn^{4+} ions with Cr^{3+} ions. In this study, this partial substitution was done with the objectives of creating Li^+ interstitial ions to form structures with general formula $Li_{1+x}Cr_xSn_{2-x}P_3O_{12}$ where $Sn^{4+} \rightarrow Li^+ + Cr^{3+}$ with x ranging from 0.1 to 0.9.

2. Experimental Procedure

2.1 Synthesis of $Li_{1+x}Cr_xSn_{2-x}P_3O_{12}$

$Li_{1+x}Cr_xSn_{2-x}P_3O_{12}$ (x = 0.1, 0.3, 0.5, 0.7, 0.9) samples were synthesized via water based citric-acid assisted sol-gel method. All the chemicals were of analytical grade and directly used as received without further purification. The starting materials used were lithium acetate (CH_3COOLi), stannum (IV) chloride pentahydrate ($SnCl_4.5H_2O$), chromium (III) acetate ($C_8H_{16}Cr_2O_{10}$) and ammonium phosphate ($H_{12}N_3O_4P$). Citric acid ($C_6H_8O_7$) acted as chelating agent and distilled water as the solvent. Firstly, CH_3COOLi, $SnCl_4.5H_2O$, $C_8H_{16}Cr_2O_{10}$ and $H_{12}N_3O_4P$ were dissolved in distilled water under magnetic stirring. Citric acid ($C_6H_8O_7$), poly ethylene glycol ($C_2H_6O_2$) and ammonium hydroxide (NH_4OH) were then mixed together to the previously prepared

solution under magnetic stirring. $C_2H_6O_6$ and NH_4OH were added to promote polyesterification and polycondensation reactions. The molar ratio of $C_2H_6O_6$ to NH_4OH was 1:1. Then, the solution was transferred into a reflux system and continuously stirred until homogenous solution was formed. After stirring for 24 hours, the solution was taken out and vaporized for about 5 hours under magnetic stirring at 80°C. The resulting gel formed was then dried in an oven at 150°C for 24 hours resulting in precursor powder. The obtained precursor powder was then ground for 30 minutes in order to obtain a very fine powder. Then, the precursor powder was subjected to sintering process at 600 °C for 48 hours. The final product was then ground again for 30 minutes before the powder was pressed using Specac hydraulic press under a pressure of 5 tons to form pellets with a diameter of 13 mm and thickness of 1.00 - 3.00 mm respectively.

2.2. Characterization Techniques

Structural analysis of the samples was performed by XRD using a PaNalytical – X'pert^3 x-ray diffractometer with Cu-K_α radiation of wavelength of 1.5406 Å. The 2θ range was between 10 ° and 45 ° and 0.026 ° in step size. Ionic conductivities of solid electrolytes are usually determined using electrochemical impendence spectroscopy (EIS). Impedance measurements of the samples were determined by AC impedance spectroscopy using Solatron 1260 Impedance Analyzer over a frequency range from 1 to 10 MHz with an applied voltage of 200 mV at room temperature. The ionic transference number measurement was evaluated by Wagner's DC polarization technique. The highest conducting sample was sandwiched between two stainless steel blocking electrodes and polarized by applying a potential of 0.5 V and the current was monitored as a function of time until it reached a steady sate condition using Wonatech ZIVE MP2 multichannel electrochemical workstation. Finally, LSV was used to study the electrochemical stability windows of the electrolytes system using Wonatech ZIVE MP2 multichannel electrochemical workstation. LSV measurement was carried out with the configuration of the cell was Li/Solid electrolytes/SS at a scan rate of 5 mV s^{-1} at room temperature.

3. Results and Discussions

3.1. Structural Properties

Figure 1 shows the X-ray diffraction patterns of $Li_{1+x}Cr_xSn_{2-x}P_3O_{12}$ (x = 0.1, 0.3, 0.5, 0.7, 0.9) samples. The XRD patterns indicate the presence of rhombohedral ($R\bar{3}c$) $LiSn_2P_3O_{12}$ crystalline phase in all the samples. SnO_2 impurity is also observed in all samples indicating the presence of unreacted cassiterite SnO_2 [17]. To confirm the Cr^{3+} ion is in the $LiSn_2P_3O_{12}$structure, the peaks in 2θ range 24°- 25° were carefully analyzed for the sample x = 0.1, 0.5 and 0.9 and the magnified XRD patterns in this 2θ range are shown in Figure 2. As seen in this figure, the peak shifts to higher diffraction angle when Cr^{3+} ion is substituted into the parent structure indicating that Cr^{3+} ion is in the $LiSn_2P_3O_{12}$ structure rather than forming impurities.

Then, the lattice parameters of the samples were calculated using the formulae that belongs to the rhombohedral crystal system with a hexagonal unit cell lattice [21, 22]

$$\frac{1}{d^2} = \frac{4}{3}\left(\frac{h^2+hk+k^2}{a^2}\right) + \frac{l^2}{c^2} \quad (1)$$

Crystallite size of the samples are determined from Scherer equation [21, 22]

$$D = \frac{k\lambda}{\beta cos\theta} \quad (2)$$

where k is the Scherer constant value (0.94), λ is the wavelength of the source (1.5406 $\dot{A}$), β is FWHM (in radians), and θ is the Bragg angle (in radians).

Meanwhile, the variations of the lattice parameters and crystallite size for $Li_{1+x}Cr_xSn_{2-x}P_3O_{12}$ system with variation of Cr content, x are listed in Table 1. Based on the table, the value of a, c and unit cell volume (V) decreases with the increment of Cr content, x in the $Li_{1+x}Cr_xSn_{2-x}P_3O_{12}$ system. The decrease in the lattice constants is attributable to the substitutions of smaller volume of Cr^{3+} ion (0.62 Å) compared to Sn^{4+} ion (0.65 Å). The substitution of stannum by chromium which results in shrinkage of unit cell volume increases the stability of the $Li_{1+x}Cr_xSn_{2-x}P_3O_{12}$ system structure [23]. However, as the Cr content, x increases the crystallite size of the system also increases.

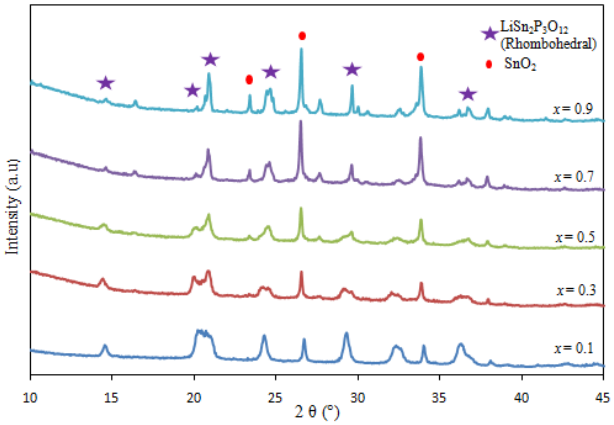

Fig. 1: X-ray diffraction patterns of $Li_{1+x}Cr_xSn_{2-x}P_3O_{12}$ system with variation of x.

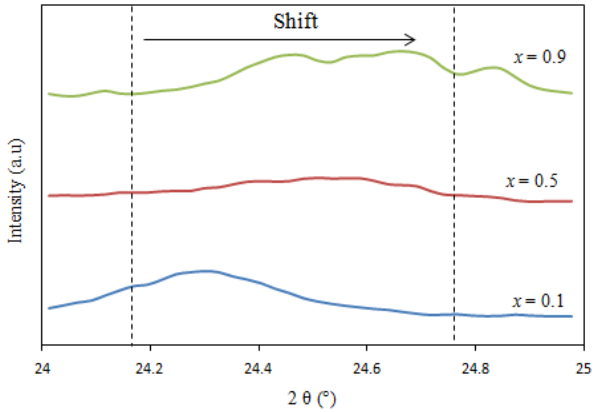

Fig. 2: X-ray diffraction patterns of $Li_{1+x}Cr_xSn_{2-x}P_3O_{12}$ system in 2θ range from 24° to 25°

Table 1*:* Lattice parameters, unit cell volume and crystallite size for $Li_{1+x}Cr_xSn_{2-x}P_3O_{12}$ system with variation of x

Samples	a [$\dot{A}$]	c [$\dot{A}$]	V [$\dot{A}^3$]	Crystallite size [$\dot{A}$]
x = 0.1	8.5078	22.0148	1341.37	138.3
x = 0.3	8.4071	21.8805	1340.17	139.9
x = 0.5	8.4069	21.8220	1336.43	140.8
x = 0.7	8.4058	21.6940	1328.35	142.4
x = 0.9	8.3704	21.5700	1309.67	144.5

3.2 DC Conductivity

The room temperature complex impedance plots of $Li_{1+x}Cr_xSn_{2-x}P_3O_{12}$ system with x = 0.1, 0.7 and 0.9 are displayed in Figure 3. From Figure 3, for $Li_{1+x}Cr_xSn_{2-x}P_3O_{12}$ system, the plots consist of two semicircles in high and intermediate frequency region with low frequency region being denoted by a spike as be seen in Figure 4 for sample with x = 0.7. The same trend also applied for x = 0.3 and 0.5. The spike at the low frequency region of all samples may indicate the effects of electrode polarization as a result of the

accumulation of ions between the electrode and the sample [24]. The high frequency semicircle is assigned to bulk response with its intercept at the *x*-axis assigned to bulk resistance, R_b, while the middle frequency semicircle is assigned to grain boundary response with its intercept at the *x*-axis corresponds to grain boundary resistance, R_{gb}. When the value of *x* increases to 0.7, both bulk and grain boundary resistances, R_b and R_{gb} shifts towards lower value indicating an increase in ionic conductivity. However, when x = 0.9, both bulk resistance, R_b, and grain boundary resistance, R_{gb} shifts towards higher value indicating a decrease in conductivity.

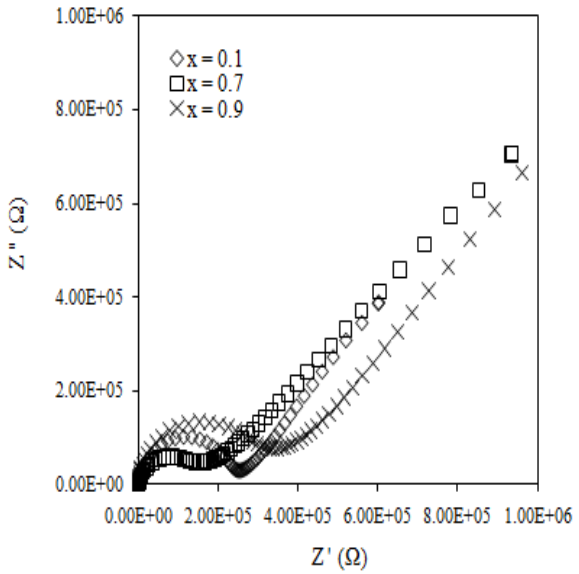

Fig. 3: Complex impedance plot of x = 0.1, 0.7 and 0.9

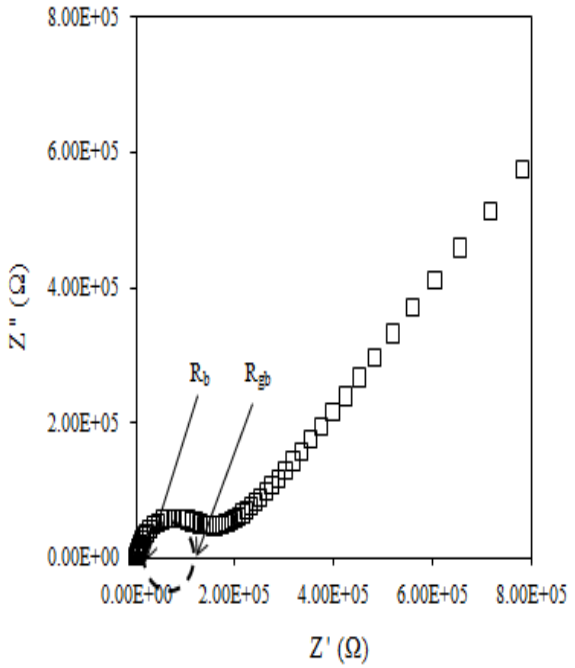

Fig. 4: Complex impedance plot of x = 0.7

Furthermore, experimental complex impedance data at room temperature may well be approximated by an equivalent circuit composed of bulk and grain boundary resistance R_b and R_{gb} and bulk and grain boundary capacitance, C_b (CPE), C_{gb} (CPE) and $CPE_{blocking\ electrode}$ with constant phase element (CPE) behaviour [25] as in Figure 5.

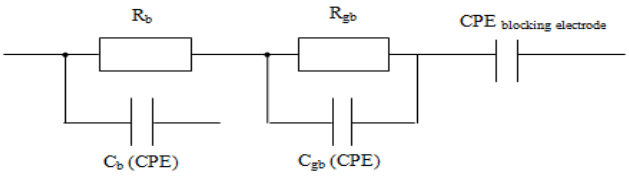

Fig. 5: Equivalent circuit of $Li_{1+x}Cr_xSn_{2-x}P_3O_{12}$ system based on impedance analysis at room temperature

Bulk and grain boundary conductivities, σ_b and σ_{gb} are then calculated using R_b and R_{gb} values determined from the impedance plots using equation:

$$\sigma_b = \frac{d}{AR_b} \quad \text{and} \quad \sigma_{gb} = \frac{d}{AR_{gb}} \tag{3}$$

The data of bulk, grain boundary and total conductivities with variation of chromium content, *x* are tabulated in Table 2.

Table 2: Bulk, grain boundary and total conductivities with the variation of chromium content, *x* at room temperature

Sample	σ_b, (S cm^{-1})	σ_{gb} (S cm^{-1})	σ_t (S cm^{-1})
x = 0.1	3.97 ×10^{-6}	1.10 ×10^{-6}	8.62×10^{-7}
x = 0.3	4.38 ×10^{-6}	1.11 ×10^{-6}	8.83×10^{-7}
x = 0.5	4.40 ×10^{-6}	1.57 ×10^{-6}	1.16 ×10^{-6}
x = 0.7	6.52 ×10^{-6}	1.62 ×10^{-6}	1.30 ×10^{-6}
x = 0.9	1.79 ×10^{-6}	1.04 ×10^{-6}	6.55 ×10^{-7}

It is observed that bulk, grain boundary and total conductivities for x = 0.1 to x = 0.7, increases with the increment of chromium content, *x*. However, when x = 0.9, the bulk, grain boundary and total conductivities decrease. The highest bulk, grain boundary and total conductivities of $Li_{1+x}Cr_xSn_{2-x}P_3O_{12}$ system at room temperature was found when x = 0.7. The highest value obtained for the grain boundary and total conductivity at room temperature in this system was two order of magnitude higher compared to the unsubstituted parent compound [9] and higher than those reported by Norhaniza et. al (2012). Therefore the increase of total ionic conductivity in the samples with excess Li mainly originates from grain boundary conductivity and not from bulk conductivity. This may be due to the ionic conductivity across grain boundaries correlates with the increased density of the pellets that takes place upon Cr substitution [23]. The increase in conductivity with Cr substitution also may be due to increase in the number of interstitial Li^+ ions due to increase in the amount of Cr^{3+} ions [26]. Besides that, another factor that contributed to bulk conductivity enhancement was the increase in crystallinity as *x* increases in the system [26]. According to Fu [27], the enhancement in crystalline phase favors high ion conduction due to the presence of larger conduction pathways for Li^+ ions migration. A similar observation also has been reported by Chowdari et al. [28]. The change in lattice parameter can also contribute to conductivity enhancement since it changes the bottleneck size and results in easy mobility of ion thus increase the ionic conductivity of the system [29]. In this work, the maximum conductivity found in the system of $Li_{1.7}Cr_{0.7}Sn_{1.3}P_3O_{12}$, was ($\sigma_b$ = 6.52 ×10^{-6} S cm^{-1}, σ_{gb} = 1.62 ×10^{-6} S cm^{-1}) at room temperature. However, we expect the ionic conductivity to increase as we increase the temperature up to 500 °C in our further study.

3.3. AC Conductivity

AC conductivity values are determined from the dielectric data as discussed in [8]. Figure 6 displays log σ_{AC} vs log ω plots of a $Li_{1+x}Cr_xSn_{2-x}P_3O_{12}$ system with x = 0.1 to 0.9. The plot consists of a plateau in intermediate frequency region and high frequency dispersion. The intermediate frequency plateau is due to frequency independence of conductivity corresponding to DC conductivity. The transition from the DC plateau to AC conductivity dispersion region shifts towards higher frequency range when value of *x* in-

creases. At high frequencies, σ_{ac} increases linearly with frequency obeying the empirical law of frequency dependence given by power law [30].

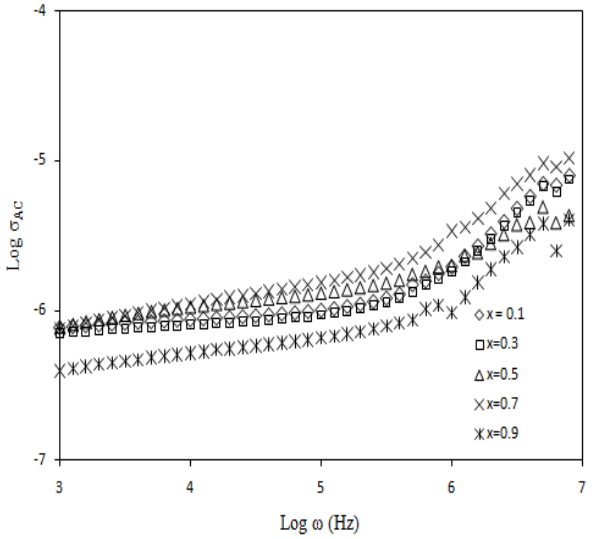

Fig. 6: AC conductivity spectra of x = 0.1 to x = 0.9

AC conductivity spectra can also be used to estimate the ionic hopping rate, ω_p in the prepared system. The ionic hopping rate, ω_p can be determined from the graph of log σ_{AC} versus log ω by extrapolating at twice the value of DC conductivity from the vertical axis horizontally towards the graph and then extrapolating downwards vertically to the horizontal axis [8]. Meanwhile, the relation of ionic hopping rate, ω_p and the magnitude of the charge carrier concentration, K then can be obtained using the following equation [28-29; 31-32]

$$K = \frac{\sigma T}{\omega_p} \tag{3}$$

where

$$K = ne^2a^2\gamma k^{-1} \tag{4}$$

In Equation 4, e is electron charge, γ is correlation factor which is set equal to 1, k is the Boltzmann constant and a is the jump distance between two adjacent sites for the ions to hope which is set to 3Å for all the samples [28-29; 32]. Next, the density of mobile ions (charge carrier), n also can be calculated using Equation 4. Next, the ionic mobility, μ can be calculated using the following equation:

$$\mu = \frac{\sigma_{dc}}{ne} \tag{5}$$

Table 2 listed all the values of ω_p, K, n, and μ for $Li_{1+x}Cr_xSn_{2-x}P_3O_{12}$ system with x ranging from 0.1 to 0.9. From the table, K values are found to be constant over x in the range of 10^{-10} Scm^{-1} KHz^{-1}. As the value of x increases up to x = 0.7, the value of n is found to be increasing indicating that all the ions which are responsible for the conductivity are in a mobile state [28 - 29]. Hence, the conduction mechanism in the investigated $Li_{1+x}Cr_xSn_{2-x}P_3O_{12}$ system is mainly attributed to the hopping of charge carriers. Meanwhile, μ also increases with the increasing of chromium content, x up to x = 0.7. This means that the increase in conductivity in the samples can be attributed to the increase in ionic mobility [28 -29]. The trend of μ value can be correlated with the results from impedance analysis showing that the $Li_{1+x}Cr_xSn_{2-x}P_3O_{12}$ system with x = 0.7 showed the highest ionic conductivity value and also possessed the highest ionic mobility, μ that is 1.74×10^{-10} cm^2 V^{-1} s^{-1}.

Table 2: Parameters of ω_p, K, n and μ for various composition of chromium content, x.

Sample	ω_p (Hz)	K (Scm^{-1} KHz^{-1})	n (cm^{-3})	μ (cm^2 V^{-1} s^{-1})
x = 0.1	7.08×10^5	4.71×10^{-10}	1.76×10^{23}	3.90×10^{-11}
x = 0.3	1.00×10^6	3.64×10^{-10}	1.36×10^{23}	5.51×10^{-11}
x = 0.5	2.51×10^6	1.81×10^{-10}	6.77×10^{22}	1.38×10^{-10}
x = 0.7	3.16×10^6	1.59×10^{-10}	5.96×10^{22}	1.74×10^{-10}
x = 0.9	5.01×10^5	6.05×10^{-10}	2.26×10^{23}	2.76×10^{-11}

3.4. Transference Number Measurement

Figure 7 shows a plot of normalized polarization current versus time for the highest conducting sample where x = 0.7. In Wagner's DC polarization technique, the ionic transference number was calculated from polarization current versus time plot using the following equation:

$$\tau_{ion} = \frac{I_{initial} - I_{final}}{I_{initial}} \tag{6}$$

where $I_{initial}$ is the initial current and I_{final} is the final residual current. From the graph, the total ionic transference number found is 0.99 and close to unity. Meanwhile, the polarization current is saturated after about 500 s. This shows that the conductivity of the $Li_{1+x}Cr_xSn_{2-x}P_3O_{12}$ system when x = 0.7 was predominantly ionic and was expected to be that of Li^+ ions.

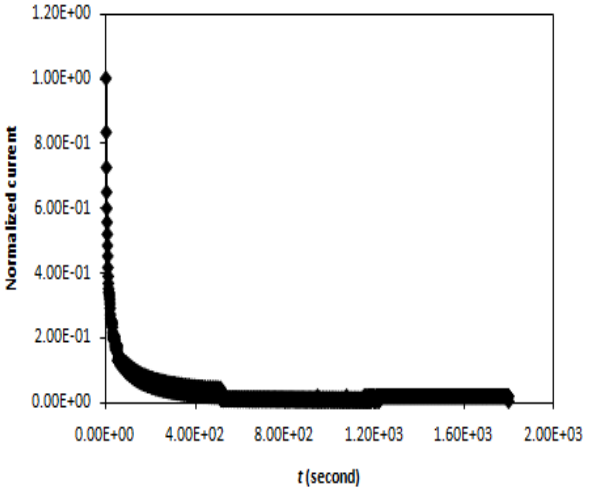

Fig. 7: Plot of normalized polarization current versus time for x = 0.7

4. Conclusion

NASICON type rhombohedral ($R\bar{3}c$) $Li_{1+x}Cr_xSn_{2-x}P_3O_{12}$ solid electrolytes with x ranging from 0.1 0.9 were obtained by water based citric acid assisted sol-gel method. XRD analysis showed that Cr^{3+} was successfully inserted into the $LiSn_2P_3O_{12}$ structure. The value of a, c and unit cell volume (V) decreased with the increment of Cr content, x in the $Li_{1+x}Cr_xSn_{2-x}P_3O_{12}$ system. The substitution of Sn^{4+} by Cr^{3+} which results in shrinkage of unit cell volume increases the stability of system structure. Furthermore, the crystallite size also increased as x increases as confirmed by the XRD analysis. The Cr^{3+} substitution also resulted in conductivity enhancement up to two orders of magnitude higher compared to the unsubsituted $LiSn_2P_3O_{12}$ at room temperature. The highest bulk, grain boundary and total conductivities found was when x = 0.7 correlated with the highest ionic mobility calculated from AC conductivity analysis. Ionic transference number value for $Li_{1+x}Cr_xSn_{2-x}P_3O_{12}$ system also close to unity that is 0.99 and suggested that the conductivity of the $Li_{1+x}Cr_xSn_{2-x}P_3O_{12}$ system was predominantly ionic and was expected to be of Li^+ ions.

Acknowledgement

The authors would like to extend their gratitude towards University of Malaya for allowing this research to be carried out. This work was supported by the Fundamental Research Grant Scheme, FP006-2013B by Ministry of Higher Education Malaysia and Lestari Grant, 600-IRMI/MyRA 5/3/Lestari (050/2017) by Universiti Teknologi MARA.

References

[1] Takada, K., "Progress in solid electrolytes toward realizing solid-state lithium batteries", *Journal of Power Sources*, Vol 394 (2018) pp 74-85.

[2] Hong, H.Y.P., "Crystal structures and crystal chemistry in the system $Na_{1+x}Zr_2Si_xP_{3-x}O_{12}$", *Materials Research Bulletin*, Vol 11, No 2, (1976) pp 173-182.

[3] Goodenough, J.B., H.Y.-P. Hong, and J.A. Kafalas, "Fast Na^+-ion transport in skeleton structures", *Materials Research Bulletin*, Vol 11, No 2, (1976) pp 203-220.

[4] Aono, H. , Sugimoto, E. , Sadaoka, Y. , Imanaka, N, and Adachi, G. "Ionic conductivity and sinterability of lithium titanium phosphate system", *Solid State Ionics*, Vol 40, (1990) pp 38-42.

[5] Hallopeau, L., Bregiroux, D., Rousse, G., Portehault, D., Stevens, P., Toussaint, G., and Laberty-Robert, C, "Microwave-assisted reactive sintering and lithium ion conductivity of $Li_{1.3}Al_{0.3}Ti_{1.7}(PO_4)_3$ solid electrolyte" *Journal of Power Sources*, Vol 378 , (2018), pp 48-52.

[6] Ramar, V., Kumar, S., Sivakkumar, S. R., and Balaya, P., "NASICON-type La^{3+}substituted $LiZr_2(PO_4)_3$ with improved ionic conductivity as solid electrolyte", *Electrochimica Acta*, Vol 271, (2018), pp120-126.

[7] Zhang, Y., Chen, K., Shen, Y., Lin, Y., and Nan, Ce-W, "Enhanced lithium-ion conductivity in a $LiZr_2(PO_4)_3$ solid electrolyte by Al doping", *Ceramics International*, Vol 43, (2017), pp S598-S602.

[8] Mustaffa, N.A., Adnan, S. B. R. S., Sulaiman, M., and Mohamed, N. S., "Low-temperature sintering effects on NASICON-structured $LiSn_2P_3O_{12}$ solid electrolytes prepared via citric acid-assisted sol-gel method" , *Ionics*, Vol 21, No 4, (2015) pp 955-965.

[9] Mustaffa, N. A. and Mohamed, N. S. , "Properties of stannum-based Li-NASICON-structured solid electrolytes for potential application in electrochemical devices", *Int J Electrochem Sci*, Vol 10, (2015), pp 5382-5394.

[10] Mustaffa, N.A., and Mohamed, N. S., "Zirconium-substituted $LiSn_2P_3O_{12}$ solid electrolytes prepared via sol–gel method", *Journal of Sol-Gel Science and Technology*, Vol 77, No 3, (2016), pp 585-593.

[11] Fergus, J.W., "Ion transport in sodium ion conducting solid electrolytes", *Solid State Ionics*, Vol 227, (2012) pp. 102-112.

[12] Knauth, P., "Inorganic solid Li ion conductors: An overview", *Solid State Ionics*, Vol 180, No 14, (2009) pp 911-916.

[13] Padma Kumar, P. and S. Yashonath, "Lithium ion motion in $LiZr_2(PO_4)_3$"*The Journal of Physical Chemistry B*, Vol 105, No 29 (2001) pp 6785-6791.

[14] Martinez, A. , Rojo, J. M. , Iglesias, J. E. , Sanz, J. , and Rojas, R. M, "Formation process of $LiSn_2(PO_4)_3$, a monoclinically distorted NASICON-type structure." , *Chemistry of materials*, Vol 6, No 10 (1994) pp 1790-1795.

[15] Martinez-Juarez, A. , Rojo, J. M., Iglesias, J. E., and Sanz, J, "Reversible monoclinic-rhombohedral transformation in $LiSn_2(PO_4)_3$ with NASICON-type structure", *Chemistry of Materials*, Vol 7, No 10, (1995) pp 1857-1862.

[16] Norhaniza, R., R.H.Y. Subban, and N.S. Mohamed," Effects of Sintering Temperature on the Structure and Conductivity of $LiSn_2P_3O_{12}$ Prepared by Mechanical Milling Method", *Advanced Materials Research*, Vol 129 m- 131, (2010) pp 338 - 342.

[17] Cui, W-J. , Yi, J. , Chen, L. , Wang, C-X. , and Xia, Y-Y., "Synthesis and electrochemical characteristics of NASICON-structured $LiSn_2(PO_4)_3$ anode material for lithium-ion batteries", *Journal of Power Sources*, Vol 217, (2012) pp. 77-84.

[18] Lazarraga, M. G. , Ibañez, J. , Tabellout, M. , and Rojo, J. M., "On the aggregation process of ceramic $LiSn_2P_3O_{12}$ particles embedded in Teflon matrix", *Composites science and technology*, Vol 64, No 5, (2004) pp 759-765.

[19] Aono, H. , Sugimoto, E. , Sadaoka, Y. , Imanaka, N. , and Adachi, G, "Electrical properties of sintered lithium titanium phosphate ceramics ($Li_{1+x}M_xTi_{2-x}(PO_4)_3$, M^{3+}= Al^{3+}, Sc^{3+}, or Y^{3+})", *Chemistry Letters*, Vol 10, (1990) pp 1825-1828.

[20] Aono, H. , Sugimoto, E. , Sadaoka, Y. , Imanaka, N. ,and Adachi, G, "Electrical property and sinterability of $LiTi_2(PO_4)_3$ mixed with lithium salt (Li_3PO_4 or Li_3BO_3)", *Solid State Ionics*, Vol 47, No 3-4, (1991) pp 257-264.

[21] Jenkins, R., X-Ray Techniques: Overview, Encyclopedia of analytical chemistry. 2000: Wiley Online Library.

[22] Jenkins, R. and R.L. Snyder, Diffraction theory. Introduction to X-ray Powder Diffractometry, Volume 138, 1996, pp 47-95.

[23] Pérez-Estébanez, M., Isasi-Marín, J., Többens, D. M., Rivera-Calzada, A., and León, C., "A systematic study of Nasicon-type $Li_{1+x}M_xTi_{2-x}(PO_4)_3$ (M: Cr, Al, Fe) by neutron diffraction and impedance spectroscopy", *Solid State Ionics*, Vol 266, (2014) pp 1-8.

[24] Mariappan, C.R. and Govindaraj, G., "Conductivity and ion dynamic studies in the $Na_{4.7+x}Ti_{1.3-x}(PO_4)_{3.3-x}$ ($0 \leq x \leq 0.6$) NASICON material", *Solid State Ionics*, Vol 176, No 13, (2005) pp 1311-1318.

[25] Yadav, P. and Bhatnagar, M. C., "Structural studies of NASICON material of different compositions by sol–gel method", *Ceramics International*, Vol 38, No 2, (2012) pp 1731-1735.

[26] Xu, X. , Wen, Z. , Gu, Z. , Xu, X. , and Lin, Z., "Preparation and characterization of lithium ion-conducting glass-ceramics in the $Li_{1+x}Cr_xGe_{2-x}(PO_4)_3$ system", *Electrochemistry Communications*, Vol 6, No 12, (2004) pp 1233-1237.

[27] Fu, J., "Fast Li^+ Ion Conduction in Li_2O-Al_2O_3-TiO_2p-SiO_2-P_2O_2 Glass-Ceramics", *Journal of the American Ceramic Society*, Vol 80, No 7, (1997) pp 1901-1903.

[28] Chowdari, B. V. R. , Rao, G. V. S., and Lee, G. Y. H, "XPS and ionic conductivity studies on Li_2O–Al_2O_3–(TiO_2 or GeO_2)–P_2O_5 glass–ceramics", *Solid State Ionics*, Vol 136, (2000) pp 1067-1075.

[29] Chang, C-M. , Hong, S-H. , and Park, H-M., "Spark plasma sintering of Al substituted $LiHf_2(PO_4)_3$ solid electrolytes", *Solid State Ionics*, Vol 176, No 35, (2005) pp 2583-2587.

[30] Jonscher, A.K., Chelsea Dielectric Press, 1983, London.

[31] Almond, D.P., G.K. Duncan, and A.R. West, "The determination of hopping rates and carrier concentrations in ionic conductors by a new analysis of ac conductivity", *Solid State Ionics*, Vol 8, No 2, (1983) pp159-164.

[32] Teo, L. P. , Buraidah, M. H. , Nor, A. F. M. , and Majid, S. R., "Conductivity and dielectric studies of Li_2SnO_3", *Ionics*, Vol 18, No 7, (2012) pp 655-665.